



CHORUS

This is the accepted manuscript made available via CHORUS. The article has been published as:

Experimental realization of an incompressible Newtonian fluid in two dimensions

Zhiyuan Qi, Cheol Soo Park, Matthew A. Glaser, Joseph E. Maclennan, and Noel A. Clark

Phys. Rev. E **93**, 012706 — Published 25 January 2016

DOI: [10.1103/PhysRevE.93.012706](https://doi.org/10.1103/PhysRevE.93.012706)

Experimental Realization of an Incompressible Newtonian Fluid in Two Dimensions

Zhiyuan Qi, Cheol Soo Park, Matthew A. Glaser, Joseph E. Maclennan, and Noel A. Clark
*Department of Physics and the Soft Materials Research Center,
University of Colorado, Boulder, Colorado, 80309, USA*

The Brownian diffusion of micron-scale inclusions in freely suspended smectic A liquid crystal films a few nanometers thick and several millimeters in diameter depends strongly on the air surrounding the film. Near atmospheric pressure, the three-dimensionally coupled film/gas system is well described by Hughes/Pailthorpe/White hydrodynamic theory but at lower pressure ($p \lesssim 70$ torr), the diffusion coefficient increases substantially, tending in high vacuum toward the two-dimensional limit where it is determined by film size. In the absence of air, the films are found to be a nearly ideal physical realization of a two-dimensional, incompressible Newtonian fluid.

PACS numbers: 47.57.Lj, 83.80.Xz, 68.15.+e, 83.60.Bc

Theoretical hydrodynamics has progressed historically through the invention of a series of abstract fluids (perfect, inviscid, incompressible, and so on) that enable the tractable description of certain physical aspects of three-dimensional (3D) fluid systems [1]. Among the most useful of these idealizations has been that of the incompressible Newtonian fluid, which is used, for example, in modeling the low-Reynolds number flow of simple and weakly-associated liquids. While there are many physical realizations of such fluids in 3D, there has been none which satisfies the basic requirements of being homogeneous in density and viscosity, and obeying the laws of conservation of mass, energy, and momentum in 2D. Currently studied 2D fluids include soap films [2], which are highly compressible in-plane due their facile response to stress (resulting in thickness changes); and few-nanometer thick, freely suspended, fluid smectic liquid crystal films [3] which in contrast, by virtue of their lamellar structure, are quantized in thickness to an integral number of layers, stabilizing hydrodynamic parameters such as density and viscosity to an extent comparable to that of 3D fluids. Both systems exchange momentum and energy with a surrounding gas but, as we will show below, the low vapor pressure [4, 5] of smectic films enables the possibility of pressure reduction to the microrange regime and thereby the approach to, and study of, the ideal incompressible, isotropic, Newtonian limit of 2D fluids. The experiments on smectic films reported here explore the evolution to this hydrodynamic regime as the surrounding gas pressure is reduced and investigate the anomalies arising from reduced dimensionality in this limit.

Hydrodynamic behavior in 2D has received extensive theoretical attention [6] and is of broad interest in the context of flows with two-dimensional character in 3D systems, generated for example by wires falling in 3D viscous fluids [7] and in the large scale motion of oceans and the atmosphere [8]. There is increasing interest in the flow of 2D films *per se* in connection with understanding the dynamical behavior of defects [9, 10], textures [11, 12] and inclusions [13–15] in smectic films, and transport in biological membranes [16, 17], all of which benefit from experimental information at or near the ideal 2D fluid

limit. As an example, the recent experiments of May et al. [18] reveal a dramatic alteration of the shape dynamics of free-floating bubbles (where a 2D smectic fluid is confined to a thin spherical shell) as a result of a partial suppression of in-plane compressibility.

The coupling of an incompressible Newtonian 2D fluid to the surrounding media was first treated by Saffman and Delbrück (SD) [19], who developed a continuum hydrodynamic model to describe the mobility μ of an inclusion of radius a , in a fluid film of viscosity η , surrounded by bulk fluid of different viscosity η' . They showed that flow in the film about a moving inclusion falls off slowly within a radius on the film of characteristic dimension $l_S = \eta h / \eta'$, known as the Saffman length, and beyond this falls off more rapidly. SD treated the case $a < l_S$, finding that the mobility of the inclusion is controlled by the film viscosity and that the film exhibits 2D flow as if bounded at l_S . Hughes, Pailthorpe, and White (HPW) [20] extended SD theory to describe inclusions of arbitrary radius, showing that for large inclusions ($a > l_S$), the mobility μ is determined by friction with the surrounding fluid, exhibiting something more like 3D Stokes behavior ($\mu \sim 1/a$) [13]. Aspects of the SD/HPW predictions for such quasi-2D fluids have since been verified experimentally [13, 21–23]. In the absence of surrounding fluid the film flow behavior should be truly 2D in character, marked by extremely long-ranged hydrodynamic interactions and inclusion mobilities that depend logarithmically on system size.

In this paper, we describe the Brownian diffusion of silicone oil droplet inclusions in smectic films as the ambient air pressure is varied from atmospheric pressure (633 torr) down to 10^{-4} torr. The experiments confirm that, while at atmospheric pressure the mobilities are limited by the surrounding gas, in the high vacuum limit the hydrodynamics are controlled by film size, with a dependence of inclusion mobility on distance from the film boundary that is described well by 2D fluid theory.

Since friction from the air plays such an important role in determining the hydrodynamic behavior of inclusions in freely suspended smectic films, understanding how the inclusion-air interactions can be tuned by varying the ambient pressure is of fundamental interest. As

the air pressure is reduced, the mean free path λ of the air molecules is expected to increase. At sufficiently low pressure, the surrounding air can not be regarded simply as an incompressible, continuous fluid and the well-established SD/HPW model based on low Reynolds number hydrodynamics can no longer be used to predict the mobilities of inclusions. We will see below that as the air is removed, this system evolves from a pseudo-3D regime where coupling to the air is dominant to a regime in which the hydrodynamics are determined by confinement at the boundaries, as predicted for an ideal 2D fluid.

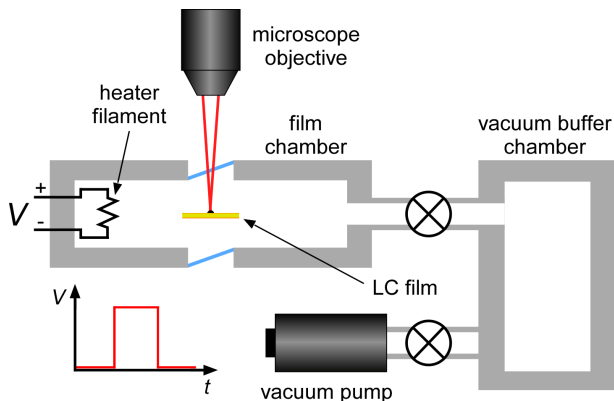


FIG. 1. (Color online) Experimental apparatus for observing inclusions in smectic liquid crystal films at low pressure. A resistive filament coated with silicone oil is briefly heated with an electric current to generate an oil vapor, part of which then condenses as droplets on the film. The buffer chamber shields the partially evacuated film chamber from sudden changes in pressure.

Homogeneous smectic films a few molecular layers thick are robust preparations [3] providing an ideal platform for studying hydrodynamics in reduced dimensions [9]. In previous experiments, we described the Brownian motion of silicone oil droplets embedded in such films with the ambient air at atmospheric pressure [15]. The oil droplets form lens-shaped [24] inclusions which are insoluble in liquid crystal and whose size remains constant over long time intervals, typically for more than half an hour, which far exceeds the time required to perform a typical measurement.

The liquid crystal material used in our experiment is 8CB (4'-n-octyl-4'-cyanobiphenyl), which is in the fluid smectic A phase at room temperature. The saturation vapor pressure of 8CB is very low (around 10^{-7} torr [4]), and we are able to maintain stable films of constant thickness over a wide range of air pressures (from atmospheric pressure to 10^{-6} torr), enabling us to study the microrheology of inclusions in the film over a wide range of reduced mean free path, given by the Knudsen number $\lambda_{\text{reduced}} = \lambda/(2R)$. The density and viscosity of 8CB are $\rho \approx 0.96 \text{ g/cm}^3$ [25] and $\eta = 0.052 \text{ Pa}\cdot\text{s}$ [26] respectively. Each smectic layer is 3.17 nm thick [27]. Freely suspended films were formed by spreading a small amount of the liquid crystal across a 4 mm-diameter hole in a glass cover

slip and the films were observed using reflected light video microscopy. The film thickness h , an integral number N of smectic layers (typically $2 \leq N \leq 6$), is determined precisely by comparing the reflectivity of the film with black glass [28]; at atmospheric pressure, the corresponding Saffman lengths are in the range $9 \lesssim l_S \lesssim 27 \mu\text{m}$. In our experimental setup (Fig. 1), a resistive filament coated in silicone vacuum pump oil (Welch 1407K DuoSeal) is then electrically heated in order to generate an oil vapor, some of which makes its way to the film where it eventually condenses and forms visible droplets, such as those shown in Fig. 2a. The droplets have radii in the range $2 \lesssim a \lesssim 50 \mu\text{m}$ and are between about 0.2 and $4 \mu\text{m}$ thick.

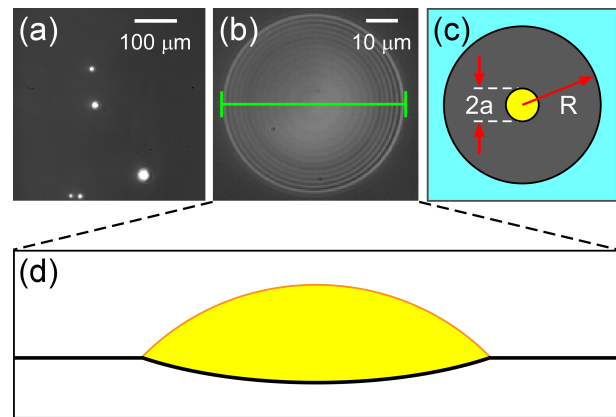


FIG. 2. (Color online) Oil droplets on smectic films. (a) Oil droplets on a three-layer, freely suspended liquid crystal film viewed in reflection. (b) Interference fringes in a large oil droplet. (c) Cartoon of an oil droplet of radius a near the center of a film of radius R . (d) Cartoon of the cross-section of an oil droplet deposited on a thin smectic film. The relative thickness of the film is greatly exaggerated here.

The shape and thickness of the oil droplets is measured by analyzing the interference fringes formed in monochromatic light (Fig. 2b) [29]. The profile of an oil droplet deposited on a film is indicated schematically in Fig. 2d. Even though the oil droplets are lens-shaped and are significantly thicker than the smectic film, they have mobilities that are described well by SD theory for flat, cylindrical inclusions of the same radius [15]. The locations of the droplet boundaries and the film edges can be determined precisely (with sub-micron resolution) by image analysis. Since the in-plane viscosity is proportional to thickness, and the background film is ultrathin, both the inclusion and the meniscus become essentially rigid within $0.5 \mu\text{m}$ or less of the film edge, effectively limiting hydrodynamic coupling to the film to a small boundary region of the thicker domains near their edges (see Appendix).

Once oil droplets appear on the film, the chamber is carefully tilted in order to maneuver a droplet of desired radius a into the center of the film (of radius R), after which the film is leveled to minimize gravitational drift. During a typical experiment, we capture several thousand

images of the film at a video frame rate of 24 fps while the droplet is in the field of view and far from the film boundaries, as shown schematically in Fig. 2(c).

After reducing the pressure of the film chamber to 10^{-4} torr, closing the valve between the pump and the vacuum buffer chamber allows us to maintain quasi-constant pressure in the film chamber for dozens of minutes, during which we are able to record the droplet motion. The pressure is then gradually increased by injecting small amounts of air into the system, allowing us to obtain a series of movies showing the Brownian motion of the droplet as the chamber pressure increases from 3×10^{-4} torr to 633 torr. These movies are decomposed into sequential images and the size and position of the droplet are determined using Canny's method for edge detection [30] and Taubin's method for object identification [31].

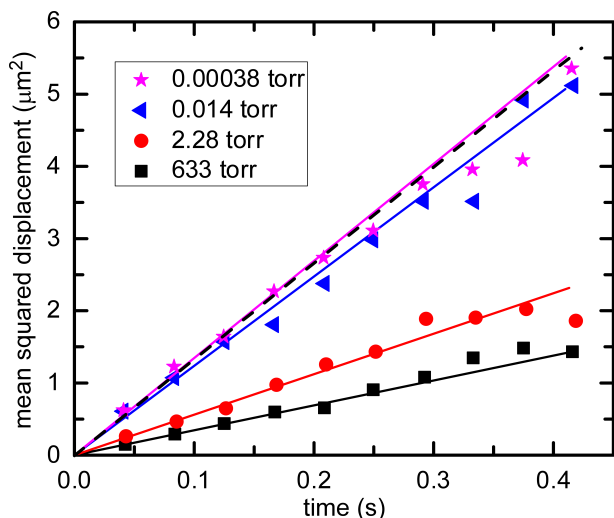


FIG. 3. (Color online) Mean squared displacement of an oil droplet ($a = 8 \mu\text{m}$) near the center of a film ($R = 2 \text{ mm}$, $N = 3$ layers) as a function of time for different surrounding air pressures (symbols). The solid lines are fits whose slopes give the corresponding diffusion coefficients. The black, dashed line is the theoretical limit corresponding to two-dimensional diffusion confined by the film boundary.

The diffusion coefficient D of a single droplet can be determined by measuring its mean squared displacement (MSD) after analytically removing any drift [13]

$$\text{MSD} = \langle (\mathbf{r}(t) - \mathbf{r}_0)^2 \rangle, \quad (1)$$

where \mathbf{r}_0 is the original position at time $t=0$, and $\mathbf{r}(t)$ the position of the particle at a later time t . Since the MSD and the diffusion coefficient D for Brownian motion in two dimensions are related [32, 33] by

$$\text{MSD} = 4Dt, \quad (2)$$

we can obtain the corresponding diffusion coefficient D by fitting the MSD vs. t data with a straight line passing through the origin, as shown in Fig. 3.

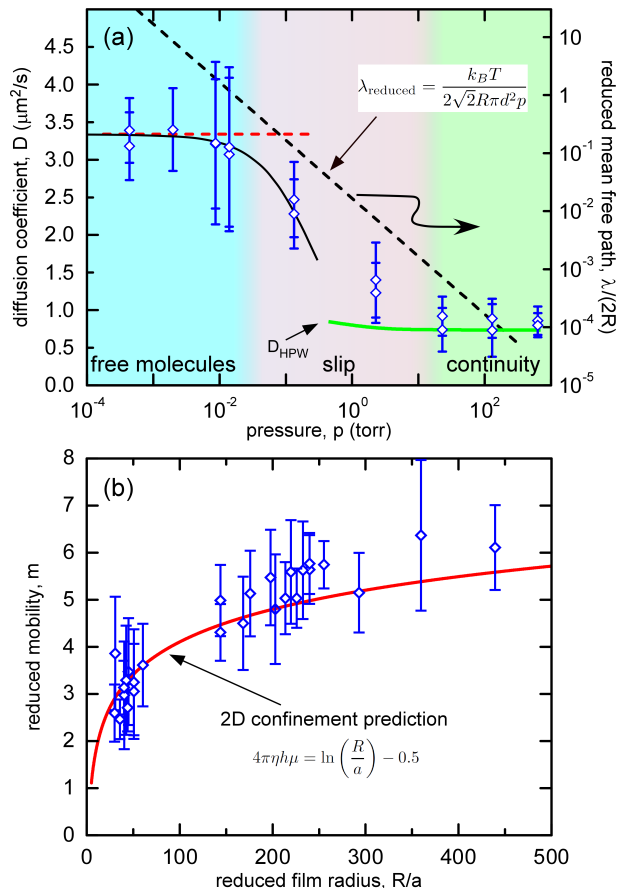


FIG. 4. (Color online) Effect of surrounding air pressure and film size on droplet diffusion. (a) Diffusion coefficient of a single droplet ($a = 8 \mu\text{m}$) near the center of a film ($R = 2 \text{ mm}$, $N = 3$ layers) as a function of surrounding air pressure (symbols). The green curve corresponds to SD/HPW theory. The black curve shows the diffusion predicted by a model assuming free air molecules impinging on the film. The horizontal dashed red line shows the 2D confinement limit predicted by Saffman for vanishingly small air viscosity and no-slip boundaries. The dashed black line shows the mean free path of the air molecules (right axis) scaled by the film diameter ($\lambda_{\text{reduced}} = \lambda/(2R)$) as a function of pressure. The background shading indicates three distinct behavioral regimes corresponding to different air pressure ranges: free molecules, slip and continuity. (b) Reduced mobility $m = 4\pi\eta h\mu$ of single oil droplets in a film in high vacuum as a function of reduced film radius. The model curve is Saffman's prediction for a 2D fluid with no-slip boundaries.

The diffusion coefficient of a typical droplet near the center of the film is plotted as a function of ambient pressure in Fig. 4(a). As the pressure is reduced from atmospheric, it is evident that the diffusion coefficient increases and eventually saturates at low pressure. At atmospheric pressure, where l_S is much smaller than the film radius R , the mobility is given by the Petrov/Schwille approximation [23] to the HPW model

$$\mu = \frac{1}{4\pi\eta h} \left[\frac{\ln(\frac{2}{\epsilon}) - \gamma + \frac{4\epsilon}{\pi} - \frac{\epsilon^2}{2} \ln(\frac{2}{\epsilon})}{1 - \frac{\epsilon^3}{\pi} \ln(\frac{2}{\epsilon}) + \frac{c_1\epsilon^{b_1}}{1+c_2\epsilon^{b_2}}} \right], \quad (3)$$

where $\epsilon = a/l_S$ is the reduced inclusion radius and $c_1 = 0.73761$, $b_1 = 2.74819$, $c_2 = 0.52119$, $b_2 = 0.61465$ are constants.

Since the viscosity of a dilute gas is independent of pressure in the hydrodynamic regime, where the molecular mean free path is small compared with the relevant feature sizes, reducing the pressure has little effect on l_S or D for pressures down to $P \approx 1$ torr (Fig. 4d). As the pressure is lowered further, however, the mean free path grows larger than the inclusion and film sizes, and the effective air viscosity falls to zero. The Saffman length, which is much smaller than R at 1 atm, thus increases as the pressure drops, becoming larger than R at sufficiently low pressure. D_{HPW} increases monotonically with increasing l_S until, in the limit $l_S > R$, the flow in the film no longer dissipates energy in the gas and the diffusion coefficient is determined by confinement by the film boundary [19]

$$D_{\text{confinement}} = \frac{k_B T}{4\pi\eta h} [\ln(R/a) - 0.5], \quad (4)$$

where k_B is the Boltzmann constant and T the temperature.

The green curve D_{HPW} shows the predictions of SD/HPW theory with the air viscosity corrected for pressure [34]. The observed variation of diffusion coefficient is well described by this model at pressures close to atmospheric ($p \gtrsim 70$ torr) but the experimental data deviate significantly from the theory at lower pressure, increasing monotonically as the pressure is reduced before saturating at very high vacuum, at the predicted limit corresponding to 2D boundary confinement (horizontal red dashed line in Fig. 4(a)). The observed behavior falls in three distinct hydrodynamic regimes: (1) Near atmospheric pressure ($p \gtrsim 70$ torr), the mean free path of the air molecules ($\lambda \sim 7 \mu\text{m}$) is much less than the diameter of the film. In this regime, the air may be regarded as a continuous fluid and diffusion is described by SD/HPW theory [13]. (2) Below about 70 torr, the viscosity of the air decreases as the pressure falls, a phenomenon attributable to slip of the air layers [34] over the surfaces of the film and oil droplet. (3) At very low pressure ($p \lesssim 0.02$ torr), the mean free path is several mm long, a distance comparable to the diameter of the film. In this regime, the ambient air can be regarded as an ensemble of collisionless molecules that obey a Maxwell-Boltzmann velocity distribution [35, 36].

In order to model the mobility of droplets at the lowest pressures, we may approximate the total drag force F as the sum of two terms, one arising from confinement by the boundaries and the other due to friction from the air, or $F = F_b + F_{\text{air}}$. The confinement term

is given by $F_b = 4\pi\eta h U / (\ln(R/a) - 0.5)$ [19]. The air drag on an inclusion moving in the film at speed U depends on both direct frictional force resulting from the impingement of air molecules on the inclusion, and on indirect frictional forces resulting from changes of streamlines in the film caused by collisions with air molecules. Calculations based on kinetic theory [37] indicate that the unit frictional force as a function of droplet speed U and surrounding air pressure p may be written $F_{\text{air}} = p\sqrt{\pi m_0 / (2k_B T)} U$, where m_0 is the mass of an air molecule. The net inverse droplet mobility may then be written as $1/\mu = 1/\mu_b + 1/\mu_{\text{air}}$. Since $\mu_b = F_b/U$ is independent of pressure, the mobility can be expressed in the form $\mu = 1/(\mu_b^{-1} + \text{const} \times p)$, where the constant can be found by fitting the experimental data at low pressure. This model is plotted as the black curve in Fig. 4(a).

In an ideal 2D fluid of finite size, therefore, the only drag experienced by a disk-like inclusion in the absence of a bounding gas should come from confinement forces arising from long-range hydrodynamic interactions with the fluid boundaries. Our experiments confirm that in high vacuum ($p \lesssim 0.003$ torr), the frictional drag from the remaining air molecules is indeed much smaller than the hydrodynamic confinement force and can be neglected. In this regime, the freely suspended SmA liquid crystal film approaches a true 2D fluid and exhibits purely 2D hydrodynamics. To verify that we were really in the 2D limit, we analyzed the Brownian motion under high vacuum of droplets of different sizes in films of different radii. The reduced mobility $m = 4\pi\eta h \mu$ of these inclusions as a function of reduced film radius R/a is plotted in Fig. 4(b). The observed mobility follows the predictions of SD theory quite well, increasing logarithmically with inclusion size as expected for a system with 2D hydrodynamic behavior. The observed mobilities are slightly larger than predicted by the model, an effect which might be due to small deviations from ideal, no-slip boundary conditions resulting from the presence of a meniscus [38] (see Appendix).

In both 3D [39, 40] and 2D fluids, inclusions near a rigid boundary experience a ‘‘wall effect’’ which reduces their mobility. In the 1940s, White studied 2D wall effects by measuring the drag on metal wires falling on their sides through viscous liquids confined between two vertical bounding plates and found that at low Reynolds number, the presence of the walls affected the mobility of the wires even when they were many hundreds of wire diameters away, with the mobility depending logarithmically on the ratio of wall separation to wire radius [7]. Recent measurements of inclusion mobility in very thick smectic films, in which the Saffman length is greater than the film size and the influence of the air is relatively small, also showed the effects of confinement by the boundary [41].

Eliminating the environmental drag on a thin smectic film by removing the ambient air seemed a promising way of studying wall effects in an ideal 2D fluid. We therefore measured the mobilities of included oil droplets

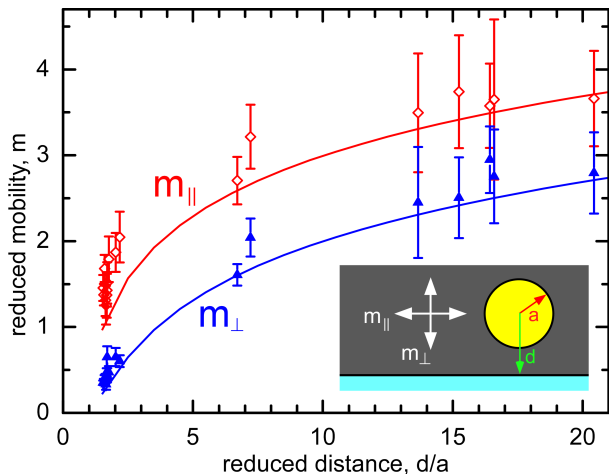


FIG. 5. (Color online) Reduced mobility of oil droplet inclusions diffusing parallel (red) and perpendicular (blue) to a straight film boundary in high vacuum. a is the radius of the inclusion and d the distance from the boundary. The model curves are analytical predictions from Eq. 5. The two mobilities show distinct behavior, as predicted by theory, increasing logarithmically with distance from the boundary as expected in 2D. In these experiments, the oil droplet radii were in the range $3 < a < 20 \mu\text{m}$.

both parallel and perpendicular to a straight boundary in high vacuum. The experimental observations, shown in Fig. 5, were compared with the model of Jeffrey and Onishi [42], who solved the Navier-Stokes equations for 2D flow around a translating cylinder a distance d from a planar boundary, assuming small Reynolds number flow. For translation respectively parallel and perpendicular to the wall, the predicted reduced mobilities are:

$$m_{\parallel} = 4\pi\eta h\mu_{\parallel} = \ln \left[\frac{d + \sqrt{d^2 - a^2}}{a} \right], \quad (5a)$$

$$m_{\perp} = 4\pi\eta h\mu_{\perp} = \ln \left[\frac{d + \sqrt{d^2 - a^2}}{a} \right] - \frac{\sqrt{d^2 - a^2}}{d} \quad (5b)$$

For large values of d/a , these expressions simplify to $m_{\parallel} \approx \ln[2d/a]$ and $m_{\perp} \approx \ln[2d/a] - 1$. In contrast to 3D fluids, where the wall effect on mobility decays within a few dozen inclusion radii [43], the influence of the boundary extends a long distance into a 2D fluid and the hydrodynamic behavior of inclusions is expected to remain anisotropic at large distances from the wall. Our experimental results confirm the predicted behavior, as seen in Fig. 5. The measured mobilities are on average slightly higher than the theory but are generally in good agreement with the model, except very close to the wall. This may be due to deviations from true no-slip boundary conditions [44] at the meniscus, as mentioned previously.

In summary, we have described the Brownian motion of single inclusions in freely suspended smectic A liquid crystal films as the pressure of the surrounding air is reduced from one atmosphere to a high vacuum. The in-

clusion mobility was characterized in three hydrodynamic regimes: near atmospheric pressure (where diffusion follows HPW theory), in partial vacuum (the slip regime), and in high vacuum (where we observe motion limited by 2D confinement effects). The parallel and perpendicular mobilities of an inclusion in high vacuum near the edge of the film increase logarithmically with distance from the boundary as predicted for an ideal 2D fluid, with an anisotropic character that persists far into the film. The observations suggest that thin, freely suspended smectic films in high vacuum are a nearly ideal experimental realization of an incompressible two-dimensional fluid. This work opens the way for more general hydrodynamic studies in this limit, of such phenomena as driven flow, high Reynolds number turbulence, energy cascades, and jets.

This work was supported by NASA Grant NNX-13AQ81G, and by the Soft Materials Research Center under NSF MRSEC Grants DMR-0820579 and DMR-1420736.

Appendix: Hydrodynamics of Boundary Regions

1. Experimental Studies of Thickness/Viscosity Near the Film-Droplet Boundary

The background 8CB films have constant layer number but the overall thickness increases substantially in the meniscus at the film boundary and at the oil drop inclusions. The inclusion and meniscus thickness, inferred from the positions of interference fringes in monochromatic light, are typically already 5 times the background film thickness within $0.5 \mu\text{m}$ of the optical edge, while the areal viscosity is typical 10 times greater, as indicated in Fig. 6.

2. Flow near the Film–Meniscus/Droplet Boundaries

The tremendous increase of the areal viscosity in the boundary regions allows the velocity field of the film to penetrate only a very short distance into the thicker regions, allowing us for all practical purposes to approximate the meniscus and silicone oil drop inclusions as being essentially solid. This assumption is justified as follows.

Since the film meniscus and oil droplet inclusions are in fact fluid objects, there will generally be some slip of the flow field of the smectic film at their boundaries. In order to evaluate how much slip there is, we consider separately the cases of transverse slip (for the component of the flow velocity parallel to the boundary) and of normal slip (for the component of the flow velocity normal to the boundary). For these purposes, we model the film/inclusion boundary as shown in Fig. 7, as a background film (smectic film, blue) in contact with a wedge of additional fluid (yellow) whose thickness increases linearly with distance from a contact line (black dot at $x = 0$) that is oriented normal to the plane of the drawing.

a. Transverse Slip

We first consider velocity $v(x)$ parallel to the boundary. We assume that everywhere on the film and in the thicker

areas there is a uniform shear force per unit length, σ , transmitted across the system in the x direction, that is constant in time and which, for $x < 0$, induces a constant transverse velocity gradient $\partial v/\partial x = \sigma/(\eta h)$. Here η is the background film viscosity and h its thickness. Transverse slip occurs when this resulting linear variation of velocity extrapolates to zero velocity at a finite distance l_{slip} beyond the contact line (Fig. 7). For $x > 0$, the system presents an x -dependent effective viscosity-thickness product, such that $\partial v/\partial x = \sigma/(\eta h + \eta_D \alpha x)$, where η_D is the viscosity of the fluid in the added (yellow) thicker wedge and α its thickness. The quantity $\eta_D \alpha x$ corresponds to the areal viscosity of the thicker wedge. Taking $v(x) = 0$ at $x = L$, with L representing the width of the meniscus or the radius of a droplet, and integrating gives the expressions for the velocity shown in Fig. 7, where $\xi \equiv \eta h/(\eta_D \alpha)$ is the characteristic distance into the droplet or meniscus by which the additional viscosity is equal to that of the background film. l_{slip} is essentially this distance, apart from a logarithmic correction that depends on L . For the typical viscosities in our experiments, we find $\xi \sim 0.02 \mu\text{m}$, which is much smaller than the optical resolution of the boundary position and thus completely negligible. This is a direct consequence of the background film being only a few nanometers thick.

b. Normal Slip

Since normal flow through the meniscus is blocked, it must be converted to transverse flow. Its penetration is then comparable to ξ , as shown in the previous section. A moving droplet, on the other hand, produces a pressure difference between its front and rear boundaries that sets up a pair of counter-rotating vortices inside the droplet as for a droplet moving in a viscous 3D fluid. These vortices circulate fluid from the front to the rear of the droplet, enabling normal flow into the boundary. In the present case, however, the effective droplet viscosity-thickness product L/ξ is more than 200 times larger than that of the background film. The corresponding reduction of velocity within the droplet forces normal flow at the boundary to be converted to transverse flow, again with a penetration length comparable to ξ .

-
- [1] H. Lamb, *Hydrodynamics* (Dover, New York, 1945).
 - [2] H. Kellay and W. I. Goldburg, Rep. Prog. Phys. **65**, 845 (2002).
 - [3] C. Young, R. Pindak, N. Clark, and R. Meyer, Phys. Rev. Lett. **40**, 773 (1978).
 - [4] J. Deschamps, J. P. Trusler, and G. Jackson, J. Phys. Chem. B **112**, 3918 (2008).
 - [5] P. Poole, C. Andereck, D. Schumacher, R. Daskalova, S. Feister, K. George, C. Willis, K. Akli, and E. Chowdhury, Phys. Plasmas **21**, 063109 (2014).
 - [6] J. Veysey, II and N. Goldenfeld, Rev. Mod. Phys. **79**, 883 (2007).
 - [7] C. White, Proc. R. Soc. A **186**, 472 (1946).
 - [8] G. Boffetta and R. E. Ecke, Annu. Rev. Fluid Mech. **44**, 427 (2012).
 - [9] C. Muzny and N. Clark, Phys. Rev. Lett. **68**, 804 (1992).
 - [10] A. N. Pargellis, P. Finn, J. W. Goodby, P. Panizza, B. Yurke, and P. E. Cladis, Phys. Rev. A **46**, 7765 (1992).
 - [11] J.-B. Lee, D. Kononov, and R. Meyer, Phys. Rev. E **73**, 051705 (2006).

- [12] P. V. Dolganov and P. Cluzeau, *Phys. Rev. E* **90**, 062501 (2014).
- [13] Z. H. Nguyen, M. Atkinson, C. S. Park, J. Maclennan, M. Glaser, and N. Clark, *Phys. Rev. Lett.* **105**, 268304 (2010).
- [14] B. Schulz, M. G. Mazza, and C. Bahr, *Phys. Rev. E* **90**, 040501 (2014).
- [15] Z. Qi, Z. H. Nguyen, C. S. Park, M. A. Glaser, J. E. Maclennan, N. A. Clark, T. Kuriabova, and T. R. Powers, *Phys. Rev. Lett.* **113**, 128304 (2014).
- [16] K. Simons and E. Ikonen, *Nature* **387**, 569 (1997).
- [17] T. T. Hormel, S. Q. Kurihara, M. K. Brennan, M. C. Wozniak, and R. Parthasarathy, *Phys. Rev. Lett.* **112**, 188101 (2014).
- [18] K. May, K. Harth, T. Trittel, and R. Stannarius, *Europhys. Lett.* **100**, 16003 (2012).
- [19] P. G. Saffman and M. Delbrück, *Proc. Natl. Acad. Sci. USA* **72**, 3111 (1975).
- [20] B. D. Hughes, B. A. Pailthorpe, and L. R. White, *J. Fluid Mech.* **110**, 349 (1981).
- [21] P. Cicuta, S. L. Keller, and S. L. Veatch, *J. Phys. Chem. B Lett.* **111**, 3328 (2007).
- [22] C. Cheung, Y. H. Hwang, X.-l. Wu, and H. J. Choi, *Phys. Rev. Lett.* **76**, 2531 (1996).
- [23] E. P. Petrov, R. Petrosyan, and P. Schwille, *Soft Matter* **8**, 7552 (2012).
- [24] C. Hui and A. Jagota, *Soft Matter* **11**, 8960 (2015).
- [25] A. J. Leadbetter, J. L. A. Durrant, and M. Rugman, *Mol. Cryst. Liq. Cryst.* **34**, 231 (1976).
- [26] F. Schneider, *Phys. Rev. E* **74**, 021709 (2006).
- [27] D. Davidov, C. R. Safinya, M. Kaplan, S. S. Dana, R. Schaetzing, R. J. Birgeneau, and J. D. Litster, *Phys. Rev. B* **19**, 1657 (1979).
- [28] E. B. Sirota, P. S. Pershan, L. B. Sorensen, and J. Collett, *Phys. Rev. A* **36**, 2890 (1987).
- [29] H. Schüring and R. Stannarius, *Langmuir* **18**, 9735 (2002).
- [30] J. Canny, *IEEE Transactions on Pattern Analysis and Machine Intelligence* (IEEE, 1986), vol. 8, pp. 679–698.
- [31] G. Taubin, *IEEE Transactions on Pattern Analysis and Machine Intelligence* (IEEE, 1991), vol. 13, pp. 1115–1138.
- [32] A. Einstein, *Annalen der Physik* **322**, 549 (1905).
- [33] A. Einstein, *Investigations on the Theory of the Brownian Movement* (Courier Corporation, 1956).
- [34] H. L. Johnston, R. W. Mattox, and R. W. Powers, *Viscosities of Air and Nitrogen at Low Pressures* (National Advisory Committee for Aeronautics, 1951).
- [35] N. A. Clark, *Phys. Rev. A* **12**, 232 (1975).
- [36] N. A. Clark, *Phys. Rev. A* **12**, 2092 (1975).
- [37] P. S. Epstein, *Phys. Rev.* **23**, 710 (1924).
- [38] F. Picano, R. Holyst, and P. Oswald, *Phys. Rev. E* **62**, 3747 (2000).
- [39] A. Banerjee and K. D. Kihm, *Phys. Rev. E* **72**, 042101 (2005).
- [40] P. P. Lele, J. W. Swan, J. F. Brady, N. J. Wagner, and E. M. Furst, *Soft Matter* **7**, 6844 (2011).
- [41] A. Eremin, S. Baumgarten, K. Harth, R. Stannarius, Z. H. Nguyen, A. Goldfain, C. S. Park, J. E. Maclennan, M. A. Glaser, and N. A. Clark, *Phys. Rev. Lett.* **107**, 268301 (2011).
- [42] D. J. Jeffrey and Y. Onishi, *Q. J. Mech. Appl. Math.* **34**, 129 (1981).
- [43] M. D. Carbajal-Tinoco, R. Lopez-Fernandez, and J. L. Arauz-Lara, *Phys. Rev. Lett.* **99**, 138303 (2007).
- [44] H. Keh and L. Wang, *J. Fluids and Structures* **24**, 651 (2008).

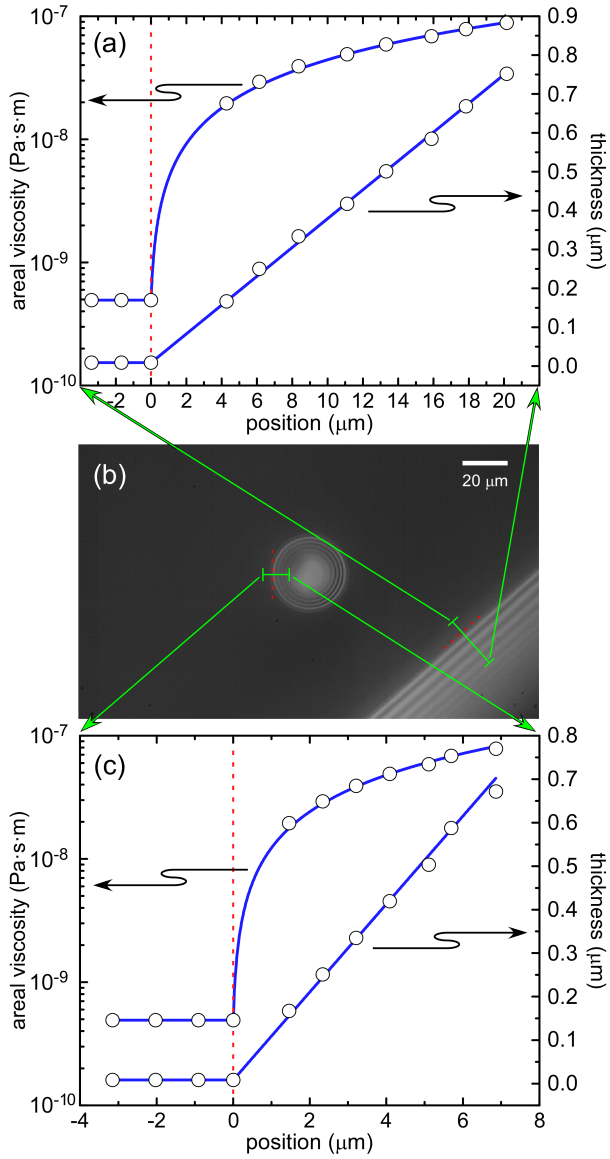


FIG. 6. (Color online) Hydrodynamic boundaries of freely suspended liquid crystal films and oil droplets. The fluid thickness and areal viscosity both increase linearly at the boundaries of the SmA film with the outer meniscus (a) and with oil droplets (c). Reflected light microscope image of a silicone oil droplet in a thin, freely suspended liquid crystal film near the meniscus at a straight boundary. The fringes are from optical interference caused by a steady increase in thickness (a and c, right). The effective viscosity in both the meniscus and the oil drop increases by several orders of magnitude within a short distance of the film boundary (a and c, left). The boundaries are indicated here by dashed red lines. Note that the viscosity and thickness are plotted on logarithmic and linear scales respectively.

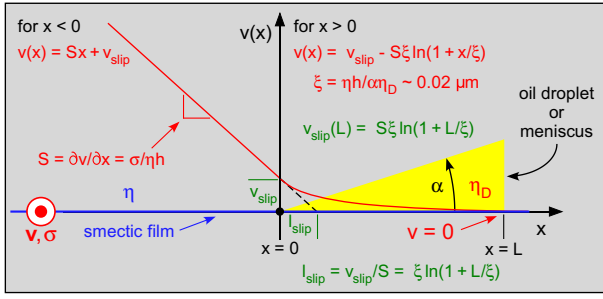


FIG. 7. (Color online) Film velocity profile near a boundary. The transverse velocity v in the film (blue region, $x < 0$) falls off linearly on approaching an oil droplet or the film meniscus, penetrating a distance l_{slip} into the thicker region (yellow wedge, $x > 0$). The velocity normal to the boundary is identically zero. The smectic film and meniscus/droplet have viscosities η and η_D respectively.